UNDERSTANDING THE ROLE OF METAL SOLUBILITY IN CONTROLLED RELEASE OF ALKALINITY USING PARTICLE-CONTAINING, OIL-IN-WATER EMULSIONS

An Honors Thesis Submitted to:
Department of Civil and Environmental Engineering

May, 2011

Olivia Leach

Committee: Prof. C. Andrew Ramsburg (Chair)
Prof. Steven Chapra
Prof. Anne Marie Desmarais

Tufts University
Medford, Massachusetts

ACKNOWLEDGEMENTS

I wish to thank Professor C. Andrew Ramsburg, as chair of my thesis committee, for his invaluable guidance throughout this research project. I am also grateful for the assistance and suggestions provided by Professor Steven Chapra and Professor Anne Marie Desmarais. Additionally, essential instruction and guidance during the research process were provided by Dr. Yongang Wang, Rhiannon Ervin, and Kate Merriam.

Support for this project was provided by the National Science Foundation through Grant CMMI 1000714, of which Professor Ramsburg is the PI. Additional support was provided in the form of a Cataldo scholarship awarded by the Department of Civil and Environmental Engineering of Tufts University.

TABLE OF CONTENTS

LIST OF FIGURES

LIST OF TABLES

ABSTRACT

Remediation of contaminants in the subsurface is a key environmental issue. Due to its noninvasive and cost-effective approach, an increasingly common method of subsurface cleanup is bioremediation, in which naturally-occurring microbes are stimulated to transform contaminants into benign or immobile substances. In order to create a favorable environment for these microbes, there are many factors that must be carefully controlled; these include sources of carbon, energy and nutrient availability, temperature, and pH. In situ bioremediation requires that these conditions be manipulated within the subsurface. Traditional subsurface alkalinity control methods are hindered by limited mixing and dispersion in the subsurface. Oil-in-water emulsions have potential as an in situ alkalinity release and delivery system; however the mechanisms that control this alkalinity release are not well documented.

The goal of this project was to examine how the chemistry of oil-in-water emulsions can be manipulated in order to control alkalinity release in the subsurface. The key hypothesis was that increasing oil polarity will increase the solubility of particles in oil, and thereby increase the thermodynamic force of partitioning into the aqueous phase.

Experimental methods were divided into three main objectives: stability, alkalinity release, and solubility experiments. A spectrophotometer was used to assess the stability of MgO and $CaCO_3$ particles in oil. Batch experiments were used to assess both the solubility of these particles in oil and the alkalinity release rate of these particles as a function of oil polarity. Data suggests that both MgO and $CaCO_3$ particles display sufficient stability in soybean oil for encapsulation within emulsions, and that increasing the oil polarity increases the rate of alkalinity release into the aqueous phase. Results also indicate some evidence of particle solubility increasing as a function of oil polarity; however, these solubility experiments require refinement.

1.0 BACKGROUND AND MOTIVATION FOR RESEARCH

The remediation of contaminants in the subsurface resulting from improper disposal, leaks, and spills is a significant environmental issue. Persistence of these sites is a threat to human, environmental, and biotic health. Due to its noninvasive and cost-effective approach, an increasingly common method of subsurface cleanup is bioremediation, in which naturally occurring microbes are stimulated to transform contaminants into benign or immobile substances (Aulenta et al., 2006; McDade et al., 2005). In order to create a favorable environment for the microbes employed in bioremediation, many factors must be carefully controlled; these include sources of carbon, energy and nutrient availability, temperature, and pH. In situ bioremediation often requires that these conditions be manipulated within the subsurface.

While immediate in situ pH control is relatively straightforward, sustained control of alkalinity is challenging; pH control must be tailored to the specific chemistry of the contaminant that is being remediated. The bioremediation of common contaminants (e.g., chlorinated solvents, heavy metals and radionuclides) may cause highly acidic subsurface conditions (Alvarez and Illman, 2006). The degradation of chlorinated solvents results in reductive dechlorination, in which hydrochloric acid and organic acids can build up in the treatment zone (Robinson and Barry, 2009). Equation 1 shows the reduction process of a generic chlorinated ethene (RCl).

$$\mathrm{RCl} + \mathrm{H_2} \rightarrow \mathrm{RH} + \mathrm{HCl} \qquad (1)$$

Many organisms that degrade contaminants operate in narrow ranges of pH (e.g., 6.0-8.0) (Wu et al., 2006). Therefore, in cases during which this acidic buildup is likely to exceed the natural buffering capacity of the soil, an alkalinity control system must be in place. A schematic of

subsurface processes contributing to alkalinity and acidic accumulation during bioremediation of a chlorinated ethene is shown in Figure 1.

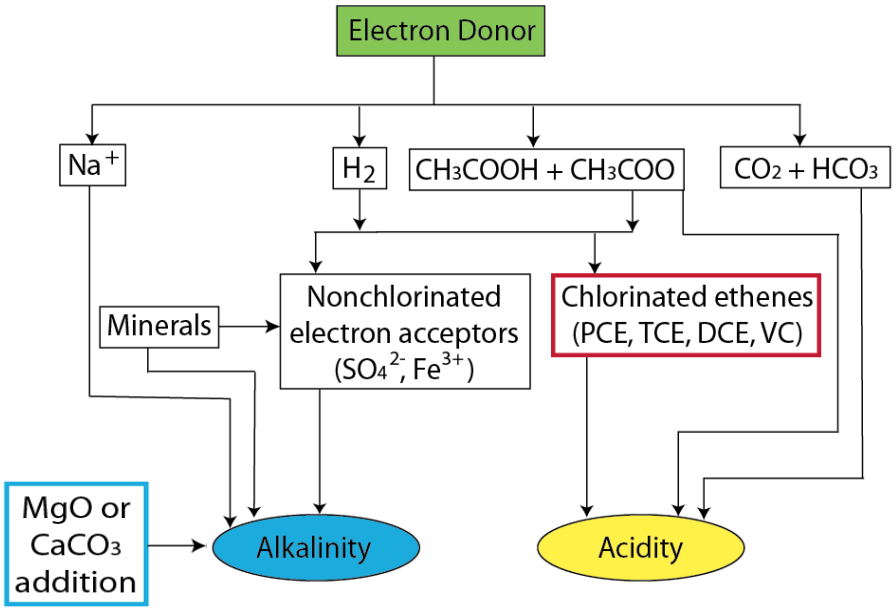

Figure 1: Schematic of subsurface processes during reductive dechlorination (adapted from Robinson et al., 2009)

Previous research has shown that adjusting subsurface pH can significantly alter microbial bioremediation rates. In one study, adjusting the subsurface pH from 4.5 to 7.4 resulted in doubling the rate of BTEX degradation (Verstraete, 1976). Shown in Figure 1 are the results of a 2006 study, in which researchers determined the effect of subsurface pH on the rate of PCE degradation by the bacteria *Dehalobacter* and *Dehalococcoides* spp. (Vainberg et al. 2006). From the figure, it is clear that the optimal pH for these bacteria appears to be between 6.0 and 6.5. A pH above or below this range significantly hinders the rate of dechlorination, and there is zero degradation at a pH of 5. A similar study in 2002 showed that TCE dechlorination rates increased significantly when pH was increased from 6.8 to 8.1 (Lee and Batchelor, 2002).

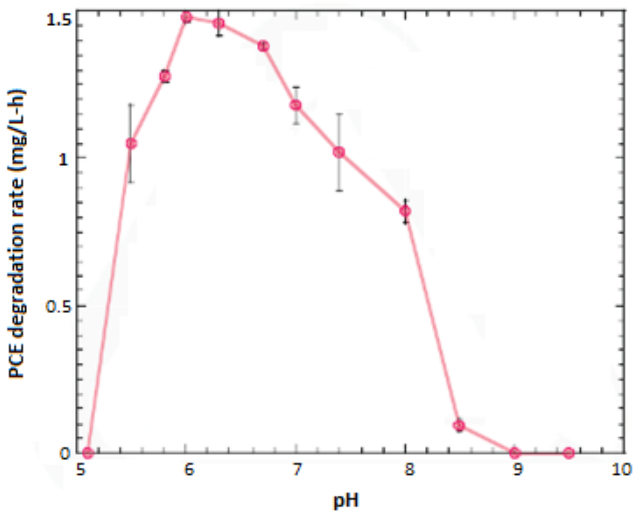

Figure 2: Effect of pH on the degradation rate of PCE by *Dehalococcoides* and *Dehalobacter* spp. (Vainberg et al. 2006)

In addition to counteracting acid buildup from degradation and optimizing the degradation rates of bacteria, there is evidence that the solubility of heavy metals such as barium, cadmium, chromium, lead, and mercury is significantly decreased when pH is increased (Dragun, 1988). These metals can therefore be precipitated and immobilized in situ by adjusting pH. Similarly, a study conducted in 2006 at the Georgia Institute of Technology found that aqueous uranium can be bioimmobilized by microbes that release phosphate (Equation 2). These researchers also found that microbial release of phosphate from these bacteria increased about 40% when the pH was increased from 5 to 7 (Martinez et al., 2006).

$$2PO_4^{2-}\,(aq) + 3UO_2^{2+}\,(aq) \rightarrow (UO_2)_3(PO_4)_2\,(s) \qquad (2)$$

Traditional techniques for manipulating subsurface pH include the addition of buffered solutions or solid alkaline material into the subsurface. These methods are hindered by limited mixing and dispersion in the subsurface; buffer capacity is quickly lost due to aqueous phase transport, as shown in Figure 2 (Arcadis, 2002; Lutes et al. 2006; Deutsch et al., 2002). It is probable that

more effective alkalinity delivery and release technologies will enhance in situ remediation processes that require pH control.

A promising technology is the use of emulsions, mixtures of normally immiscible fluids (e.g., oil and water) that are stabilized by surfactants (Enfield et al., 1999). Emulsions are widely used in the food and pharmaceutical industries as delivery systems for encapsulating, protecting, and releasing active ingredients such as bioactive lipids (McClements et al., 2007). In regards to subsurface remediation, emulsions are a common amendment for stimulation of bioremediation (Borden, 2007). Emulsions have been used in the subsurface to transport both solutes and particles used for remediation (Berge and Ramsburg, 2009; Ramsburg et al., 2003). Macroemulsions (i.e., emulsions that are thermodynamically unstable) have the potential to deliver and release alkalinity at a controlled rate as droplets travel and become immobilized within the subsurface.

Oil-in-water emulsions have a number of advantages over traditional alkalinity control techniques. Unlike aqueous buffered solutions, emulsions are not affected by aqueous-phase transport; instead, particle-containing oil-in-water emulsions interact with the solid phase in the aquifer, gradually creating a thin coat of oil droplets around soil particles (Borden et al., 2008). This coat of oil is capable of releasing alkalinity at a controlled rate as groundwater flows through the injection site, thereby creating a plume of alkalinity down-gradient of the injection well (Figure 3). The amount of oil that is retained around the solid aquifer particles is dependent on the clay content of the soil, with higher amounts of clay resulting in higher retention (Coulibaly and Borden, 2004).

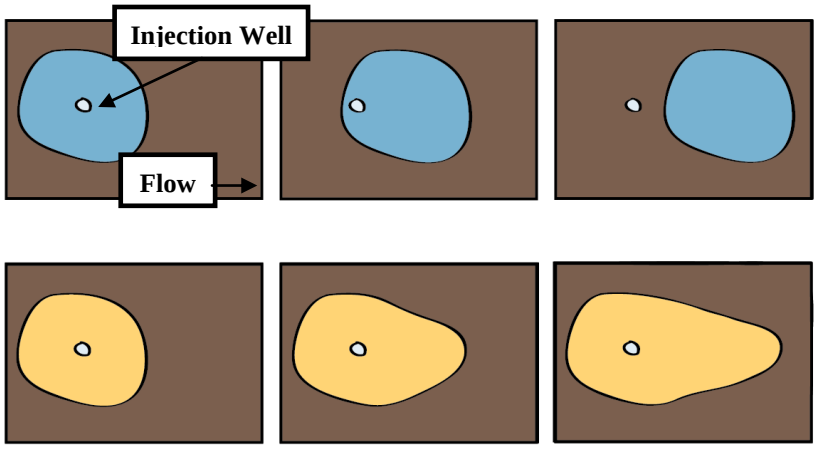

Figure 3: Theoretical effect of aqueous phase transport on buffered solution (top) and emulsion (bottom)

An additional benefit to oil-in-water emulsions is that the emulsified oil itself can be used as substrate to enhance microbial growth and proliferation during in situ enhanced bioremediation. In the subsurface, emulsified oils are fermented to H_2 and acetate; these products are then used as carbon and energy sources for microbes responsible for degradation (Borden et al., 2008). A 2006 study found that an injection of emulsified oil into a column of sand contaminated with PCE generated strongly reducing, anaerobic conditions for at least 14 months (Long and Borden, 2006). Emulsified oils have been shown to enhance the biodegradation of chlorinated ethenes, chlorinated ethanes, halomethanes, perchlorate, nitrate, some metals, and some explosives (Borden et al., 2008).

Thus, emulsions hold great promise for delivering alkalinity and sustaining microbial populations within the contaminated subsurface environment. In fact, this idea has already been brought to fruition as AquaBupH®, a commercially available pre-mixed soybean-oil and particulate suspension emulsion that is advertised to enhance dechlorination by stabilizing pH (Marlow, 2009). However, although there has been a significant amount of research regarding the transport of emulsions in the subsurface (e.g., Borden et al., 2008; Long and Ramsburg, 2011; Geiger et al. 2002), the mechanisms governing the rate of alkalinity release from these oil-

in-water emulsions are not well-documented or understood. Previous work investigating these mechanisms at Tufts University showed that alkalinity particles in the form of calcium carbonate can be stabilized in oil-in-water emulsions, and that the rate of alkalinity release from the oil to the aqueous phase varies as a function of oil polarity (Almquist, 2009). This project aims to further develop these investigations.

2.0 OBJECTIVES & HYPOTHESES

The objective of this research project was to explore the role of solution polarity in controlling the solubility of metal oxides from oil-in-water emulsions containing metal oxide nanoparticles. Sources of alkalinity for the following experiments were calcium carbonate ($CaCO_3$) and magnesium oxide (MgO) nanoparticles, provided by Acros Organics and Nanostructured & Amorphous Materials, respectively. The use of two different particle types may enable future researchers to design alkalinity release strategies for site-specific in situ remediation. Previous work has shown that metal nanoparticles can successfully be encapsulated within soybean oil droplets for targeted delivery, thus enabling the basis for this project (Crocker et al. 2008; Berge and Ramsburg, 2009; Long and Ramsburg, 2011; Almquist, 2009). Central to the work proposed here is the hypothesis that oil-in-water emulsions can be used for controlled release of alkalinity in the subsurface, and that these emulsions can be designed to release alkalinity at a rate that is proportional to acid production within the subsurface. These hypotheses were not directly tested in this research. Rather, it is anticipated that the results of this project will permit future research to explore tuning the rate of alkalinity release.

The rate of alkalinity release can be described using a linear driving force model (Equation 3), where a_i is the interfacial area between oil and water, V is the aqueous-phase volume, C is the carbonate (or metal) concentration, k_f is the mass transfer coefficient, and C^* is the effective carbonate solubility.

$$V\frac{dC}{dt} = a_i k_f (C^* - C) \qquad (3)$$

According to Equation 3, the rate of alkalinity release (dC/dt) can be increased by altering either the lumped mass transfer coefficient $(a_i k_f/V)$ or C^*. The key hypothesis of this research is

that alkalinity release from soybean oil can be controlled by modifying the polarity (i.e., dielectric constant) of the oil. Nonpolar fluids such as soybean oil are characterized by low dielectric constants. The dielectric constant of soybean oil can be modified by the addition of co-solvents (i.e., low molecular weight alcohols such as 1-butanol). Specifically, I hypothesize that increasing the polarity of the soybean oil will increase the solubility of the nanoparticles. In turn, increased solubility of these nanoparticles will increase the thermodynamic force for partitioning into the aqueous phase, thus offering control over the rate of alkalinity release.

Specific objectives of this research are: (1) test the stability of MgO and $CaCO_3$ nanoparticles in soybean oil, (2) conduct proof-of-concept alkalinity release experiments and reanalyze existing data regarding alkalinity release rate as a function of cosolvent (1-butanol) concentration, and (3) assess the solubility of MgO and $CaCO_3$ nanoparticles in soybean oil as a function of oil polarity.

3.0 EXPERIMENTAL DESIGN, MATERIALS AND METHODS

This research is divided into three main tasks: particle stability, alkalinity release rate, and particle solubility. Experiments were conducted according to the methods below. $CaCO_3$ particles were obtained from Acros Organics. MgO particles were obtained from Nanostructured and Amorphous Materials. Soybean oil was purchased from MP Biomedicals. 1-Butanol and hydrochloric acid (HCl) were supplied by Fisher Scientific. Purified water (resistivity >18.2 mΩ/cm and total organic carbon (TOC) <10 ppb) was obtained from a MilliQ Gradient A-10 station (Millipore Inc.). A summary of materials used in experiments is shown in Table 1. All materials, including standards, and instruments used in this research are also detailed in Appendix A.

Table 1: Materials

Material			Manufacturer	Grade	Physical Properties	
					Dielectric Constant (25°)	Bulk Density (g/cm^3)
Calcium Carbonate particles	99%+ purity	60nm[1]	Acros Organics	ACS	N/A	2.83
	98% purity	10µm	Sigma-Aldrich			2.93
Magnesium Oxide particles, 99%+ purity		20nm	Nanostructured & Amorphous Materials, Inc.	ACS	N/A	3.58
		50nm				
		100nm				
		~44µm	Sigma-Aldrich			
1-Butanol			Fisher Scientific	HPLC	17.8[2]	0.81
Hydrochloric acid			Fisher Scientific	HPLC	78.30[3]	1.18
Milli-Q water			Millipore	N/A	80.4[1]	0.845-0.875
Soybean oil			MP Biomedicals	Laboratory	3.3[1]	0.92
Kerosene			Sigma Aldrich	Pure	1.8[1]	0.81

[1] Almquist, 2009

[2] "Dielectric"

[3] Hydrochloric, 2010

For the purpose of this project, modified soybean oil is herein defined as soybean oil (dielectric constant of 3.3) that has been equilibrated with the cosolvent 1-butanol (dielectric constant of 17.8) and water (dielectric constant of 80.10) (Berge and Ramsburg, 2009). Modified soybean oil therefore possesses an increased water and 1-butanol content, and higher dielectric constant (i.e., polarity). The dielectric constants of these modified oils at 22±2 ºC were measured with a Brookhaven BI-870 Dielectric Constant Meter. Based on preliminary work, the target dielectric constant range for these solutions was 3.3 to 6.

3.1 Task 1: Stability Experiments

The stability of nanoparticles suspended in oil is a key factor to the success of alkalinity delivery through emulsions. Previous work has shown that iron nanoparticles can be suspended within oil-in-water emulsions (Berge and Ramsburg, 2009). These suspensions required an additional surfactant coating around the particles within the oil in order to enhance suspension stability. This work builds upon these studies, with the important distinction that, due to their nonmagnetic nature, it was hypothesized that both MgO and $CaCO_3$ particles will display adequate stability so as to not require surface coatings. The following subtasks compare different properties of particle-in-oil suspensions in order to quantify the sedimentation kinetics. From these data, time constants for $CaCO_3$ and MgO nanoparticle destabilization and sedimentation were determined using methods detailed in Subtask 1.4, below. If suspensions displayed little stability (i.e., rapid sedimentation within 10 min) then surfactants or polymer coatings would have be used to enhance the stability of the particles (e.g., Phenrat et al., 2008; Berge and Ramsburg, 2009; Long and Ramsburg, 2011).

3.1.1 Subtask 1.1: Effect of particle loading on stability

The purpose of Subtask 1.1 is to determine the effect of nanoparticle concentration on particle-in-oil suspension stability. $CaCO_3$ nanoparticles (~60nm) were massed to achieve concentrations of 0.05%, 0.10%, and 0.20% mass in soybean oil (Almquist, 2009). All suspensions were prepared with un-centrifuged, unmodified soybean oil. The particle-oil mixtures were sonicated at 100% amplitude for 1 minute with a Fisher Scientific Sonic Dismembrator (model 500) in order to enhance the stability of the suspensions. Aliquots of each suspension were then immediately transferred to a spectrophotometer cuvette. Using a PerkinElmer UV/VIS spectrophotometer (model Lambda 25), light transmission through these cuvettes was monitored for four hours at 580nm (Long and Ramsburg, 2011). Four hours was chosen as a reasonable amount of time to complete emulsion injection into the subsurface. Once injected, shear forces from the subsurface pore spaces are sufficient to ensure particle stability.

3.1.2 Subtask 1.2: Effect of particle size and type on stability

The purpose of Subtask 1.2 is to determine the effect of particle size and type on stability. To accomplish this task, the methods described in Subtask 1.1 were repeated, replacing $CaCO_3$ particles with MgO particles. In addition, each particle-in-oil suspension concentration contained a subset of three different size fractions: 20nm, 50nm, and 100nm.

3.1.3 Subtask 1.3: Effect of oil composition on stability

The purpose of Subtask 1.3 is to determine the effect of oil composition on the stability of particle-in-oil suspensions. The following experiments did not contain any particles. A cuvette containing unmodified soybean oil was monitored with a spectrophotometer at 580nm for four hours. This experiment was then repeated with unmodified soybean oil that had been centrifuged

at 2500 rpm for 10 minutes. An aliquot of the centrifuged oil was then siphoned off and monitored via spectrophotometer using the previously described methods. The goal of this experiment was to determine if the natural composition of the soybean oil was causing background interference on the stability analysis of the nanoparticles.

3.1.4 Subtask 1.4: Sedimentation data analysis

The data obtained from Subtasks 1.1 through 1.3 were transformed using a model (Equation 4) that analyzes a suspension as being comprised of settling and nonsettling fractions in order to obtain sedimentation time constants (τ). In this model, adsorption of light is assumed to be linearly related to particle concentration. A_i is the normalized absorbance of the ith settling fraction, and A_0 is the normalized absorbance of the nonsettling fraction. (Long and Ramsburg, 2011; Nicolosi et al., 2005)

$$A_T = A_0 + \sum_{i=1}^{n} A_i \exp\left(-\frac{t}{\tau_i}\right) \qquad (4)$$

The data obtained from Subtasks 1.1 and 1.2 were fit assuming one nonsettling fraction and one settling fraction. SigmaPlot was used to complete this regression analysis.

3.2 Task 2: Preliminary Rate Experiments

3.2.1 Subtask 2.1: Proof-of-concept alkalinity release experiment

The next consideration in confirming the plausibility of using these particles in alkalinity delivery systems is alkalinity release. Task 2 serves as a preliminary measure to justify continuation into Task 3, solubility experiments. Control of groundwater pH using emulsions requires effective alkalinity release from the oil phase to the aqueous phase. Proof-of-concept batch experiments were conducted with the objective of providing a preliminary assessment of

the rate of alkalinity release from nanoparticle-containing oils (modified and unmodified). Alkalinity release was quantified by measuring the pH of the aqueous phase in a closed system where interfacial area and mixing were controlled. The pH of 90 mL of acidified water at 22±2ºC (initial pH ≈ 4) beneath a layer of 10 g of oil containing a 1% particle suspension was monitored over a 24-hour period. The experimental setup is shown in Figure 4.

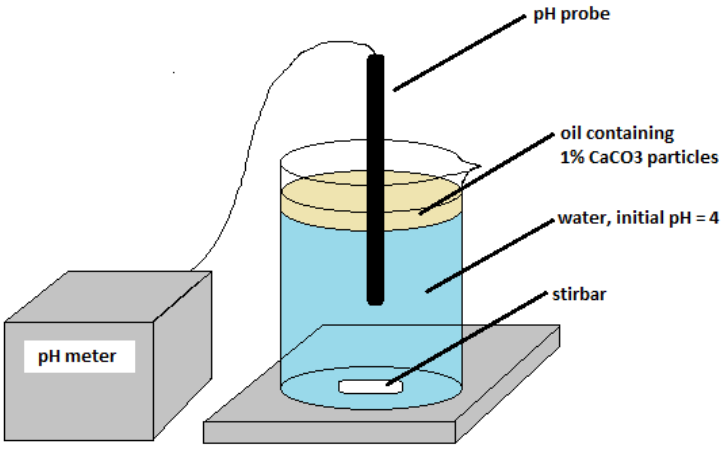

Figure 4: Experimental setup for alkalinity release experiments

3.2.2 Subtask 2.2: Analysis of existing data

The primary focus of Task 2 was reanalyzing existing data related to $CaCO_3$ alkalinity-release, obtained by the same methods as described in Subtask 2.1 (Almquist 2009). These pH vs. time data were transformed to alkalinity vs. time using Equations 5 thru 8, which are based on the assumption of a closed system (Bialkowski, 2004).

$$C_T = \frac{\Delta[OH^{-1}] - \Delta[H^+]}{2 * \alpha_0 + \alpha_1} \quad (5)$$

$$\alpha_1 = \frac{1}{1 + {[H^+]}/{K_{a1}} + {K_{a2}}/{[H^+]}} \quad (6)$$

$$\alpha_0 = \frac{1}{1 + {K_{a1}}/{[H^+]} + {(K_{a1} * K_{a2})}/{[H^+]^2}} \quad (7)$$

$$\alpha_2 = 1 - \alpha_0 - \alpha_1 \quad (8)$$

Where C_T is the carbonate concentration at the observed time in mol/L, $\alpha_0, \alpha_1, \alpha_2$ are the fractional amounts of carbonate species (H_2CO_3*, HCO_3^-, CO_3^{2-}, respectively), and K_{a1} and K_{a2} are equilibrium constants.

This total alkalinity versus time data was fit using a completely mixed batch reactor model with a source term that includes an intrinsic mass transfer coefficient (K_f), interfacial area (A), aqueous phase volume (V), and linear driving force ($Ca_{soly}^{2+} - C_T$). Using the initial pH adjustment to determine [Cl^-], the system is reduced to seven equations (electroneutrality, K_{a1}, K_{a2}, K_w, K_{sp}, and Equation 13) and seven unknowns (H_2CO_3, HCO_3^-, CO_3^{2-}, OH^-, H^+, C_T, and Ca^{2+}). Equations 9 thru 12 were obtained from temperature (T) dependencies from literature (Shadlovsky and McInnes, 1935; Harned and Hamer, 1933; Harned and Scholes, 1941).

$$K_{sp} = 10^{(-0.1183*T+8.03)} \quad (9)$$

$$K_{a2} = 10^{\left(-\frac{2902.39}{T}+0.02379*T-6.498\right)} \quad (10)$$

$$K_{a1} = 10^{\left(-\frac{17052}{T}+215.21*\log(T)-0.1275*T-545.56\right)} \quad (11)$$

$$K_w = 10^{\left(-\frac{4787.3}{T}+7.1221*\log(T)+0.010365*T-22.801\right)} \quad (12)$$

$$C_T = Ca^{2+} = Ca_{soly}^{2+}\left(1 - \exp\left(-\frac{k_f A t}{V}\right)\right) \quad (13)$$

Equation 13 represents the integral of Equation 3, the linear driving force model. The lumped mass transfer coefficient $\left(\frac{k_f A}{V}\right)$ and Ca_{soly}^{2+} were fit to the C_T versus time data. Fits were solved for iteratively in MatLAB.

3.3 Task 3: Solubility Experiments

3.3.1 Subtask 3.1: Inductively Coupled Plasma (ICP) calibration curves

The success of Tasks 1 and 2 would justify the expansion of this project into Task 3, determining the relationship between oil polarity and metal solubility. To measure the solubility of $CaCO_3$ and MgO particles in soybean oil, metal content in solution was quantified using a Perkin Elmer Optima 7300 DV ICP-OES. The ICP measures the concentration of the metal cation associated with the particles used in a particular experiment (either Mg^{2+} or Ca^{2+}). This value was then used to calculate the solubility of the alkalinity components within the soybean oil using molar ratios from the dissolution reactions. The purpose of Subtask 2.1 was to (1) produce two aqueous calibration curves for the ICP, one each for Mg^{2+} and Ca^{2+}, (2) optimize an ICP method based on the literature for the dissolved-in-oil standards, and (3) produce ICP calibration curves for these cations dissolved in oil. ICP standards were purchased from PerkinElmer (aqueous) and AccuStandard (dissolved-in-oil).

The aqueous calibration curve was analyzed with the ICP according to the PerkinElmer Application Note: Analysis of Trace Metals in Surface and Bottled Water (Sarojam, 2010). Dissolved-in-oil standards were prepared by dilution with kerosene and soybean oil, using the methods outlined in the European standard EN 14538 (EN 2006). The initial method for analysis of the dissolved-in-oil calibration curves was based on the PerkinElmer Application Note: Phosphorus, Calcium, and Magnesium Analysis of Soybean Oil-Feedstock for Biodiesel Production Using the Optima ICP-OES (Knoll and Knopp, 2007). The instrumental parameters for both these methods are summarized in Table 2.

It should be noted that the recommendations by Perkin Elmer for ICP spray chamber and nebulizer choice (baffled cyclonic and low flow, respectively) for oil-based samples were not

available in the lab. Instead, a cross-flow nebulizer and standard spray chamber were used. Because of this, precautions were taken to avoid excessive carbon buildup during sampling.

Table 2: Preliminary Instrumentation for ICP-OES Methods from literature

Parameter	Method	
	Aqueous (Sarojam 2010)	**Dissolved-in-Oil (Knoll and Knopp 2007)**
Ca^{2+} wavelength (nm)	317.933	317.933
Mg^{2+} wavelength (nm)	285.213	285.213
Plasma Flow (L/min)	15	18
Auxiliary Flow (L/min)	0.2	1.4
Nebulizer Flow (L/min)	0.8	0.45
RF wattage (W)	1450	1500
Pump Flow Rate (mL/min)	1.5	1.5

3.3.2 Subtask 3.2: Relationship between oil polarity and particle solubility

To determine the relationship between oil polarity and nanoparticle solubility, a series of batch experiments was conducted. The solubility of MgO and $CaCO_3$ particles were assessed in aliquots of modified and unmodified soybean oil. Soybean oil was modified by equilibrating with varying proportions of 1-butanol and water for 72 hours. The water content of each aliquot of modified oil was quantified with a Mettler-Toledo Karl Fischer Titrator (Model DL38). 1-Butanol concentrations were determined using a Hewlett-Packard Gas Chromatograph (Model 5890) equipped with a Perkin Elmer headspace sampler (Model Turbomatrix 40 Trap) and a flame ionization detector. The dielectric constant of each oil solution was measured using a Brookhaven dielectric constant meter (model BI-870). Particles (>10 µm, provided by Sigma-Aldrich) were then added in excess to each aliquot of oil solution and mixed for one week. These particle-in-oil mixtures were then centrifuged using a Beckman Coulter Centrifuge (model Avanti J-25) at 2500 rpm for 10 minutes. The soybean oil was diluted with kerosene by a factor of two and sampled for the metal ions associated with the dissolution of each particle (Ca^{2+} or

Mg^{2+}), using the optimized ICP instrumentation determined by completing Subtask 3.1. In order to avoid variations in intensity readings by the ICP during sampling due to carbon buildup, new calibration curves were created after every five samples.

Solubility data was analyzed as a function of the dielectric constant of the modified oils. It was hypothesized that increasing oil polarity would increase particle solubility.

A contingent experiment for Task 3 was also performed in order to determine whether the distribution of Ca^{2+} and Mg^{2+} particles can be determined for oil-water-butanol systems at equilibrium as a function of oil polarity. To complete this experiment, particles were added in excess to water and equilibrated for 72 hours at 22±2 ºC. This water, saturated with either MgO or $CaCO_3$ particles, was then used in equilibration with varying proportions of soybean oil and 1-butanol. The hypothesis of this experiment was that metal ion partitioning could be determined as a function of oil polarity.

4.0 RESULTS & DISCUSSION

4.1 Stability Experiments

Stability experiments were completed using the methods described in Subtasks 1.1 and 1.2. Data were then transformed by normalization and used to fit (via nonlinear least-squares) the time constants (τ_i) and population fractions (A_i) associated with the model described in Subtask 1.4. Results are shown in Tables 3 and 4 with standard error for each fitting parameter. The normalized data and model fits with 95% confidence intervals are plotted in Figures 5 through 8, where A/A_0 is the absorbance at time t divided by the initial absorbance. These plots suggest that the model provides a reasonable description of the settling for the 50 and 100 nm particles sizes of MgO. The model does not capture the overall trend for the smaller MgO particles (20 nm); one hypothesis for this discrepancy is that the particles agglomerated in the oil and affected the settling rate (Figure 5). Regression on the $CaCO_3$ data could only be performed on the first 90 minutes of data, as opposed to the full four hours for the MgO particles; the fit did not converge beyond 90 minutes. From the four-hour $CaCO_3$ sedimentation curve shown in Figure 9, it is evident that the $CaCO_3$ particles display a different settling trend than the MgO particles, and thus diverged from the model.

The results from the 50 and 100 nm MgO particles confirm the model's assumption that the suspensions are comprised of one settling fraction and one nonsettling fraction. The fraction of absorbance due to the nonsettling fraction ranged from 0.945 to 0.984; therefore >94% of these suspension are stable over 4 hours. This confirms that MgO particles (50 and 100 nm) at concentrations of 0.05, 0.10, and 0.20% display adequate stability in oil due to viscous effects alone. Although the $CaCO_3$ particle settling curve did not converge to the model fit after 90 minutes, it is evident from Figure 9 that >75% of the particles are stable over the 4-hour time

period. This fraction is suitable to justify $CaCO_3$ encapsulation within emulsions. Due to the probable agglomeration of the 20nm MgO particles, it is not recommended that these particles be utilized in emulsion encapsulation.

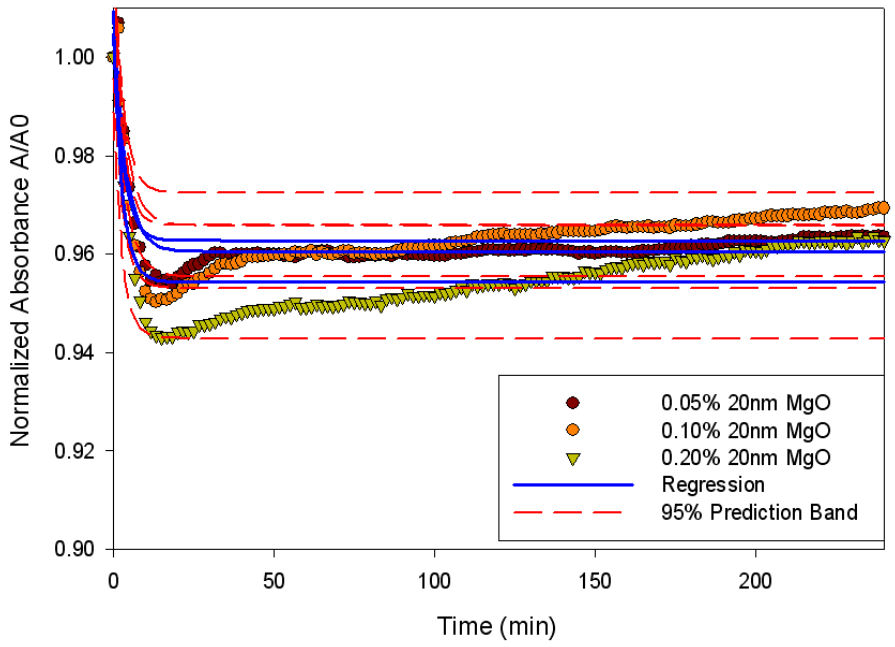

Figure 5: Normalized settling curve of 20nm MgO particles in soybean oil and corresponding regression

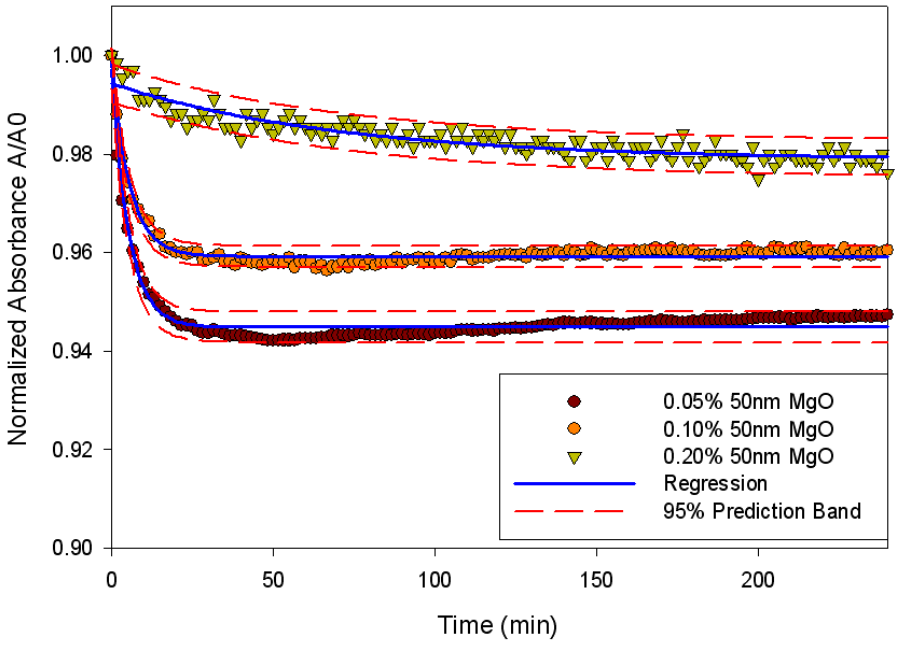

Figure 6: Normalized settling curve of 50nm MgO particles in soybean oil and corresponding regression

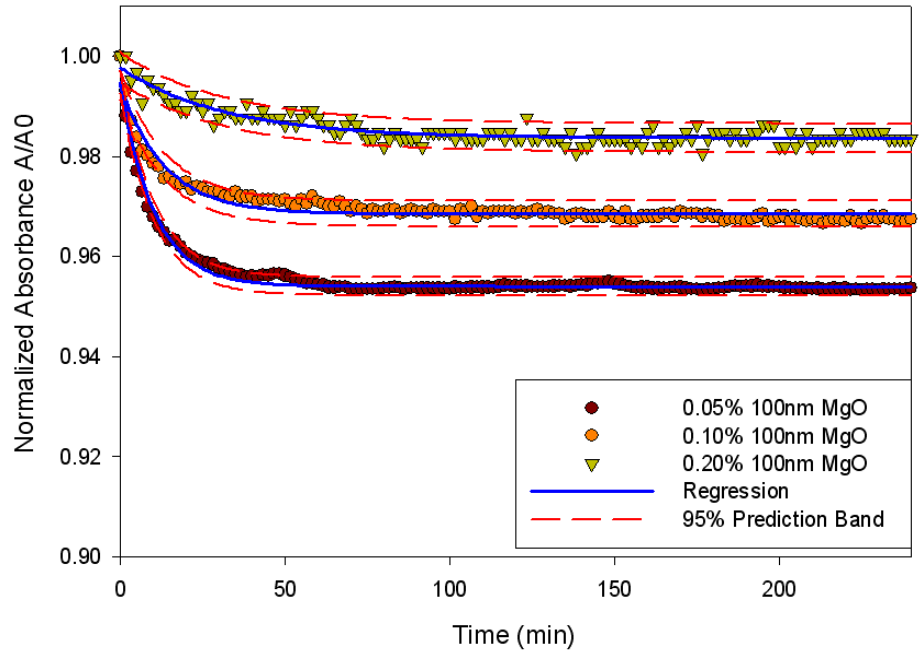

Figure 7: Normalized settling curve of 100nm MgO particles in soybean oil and corresponding regression

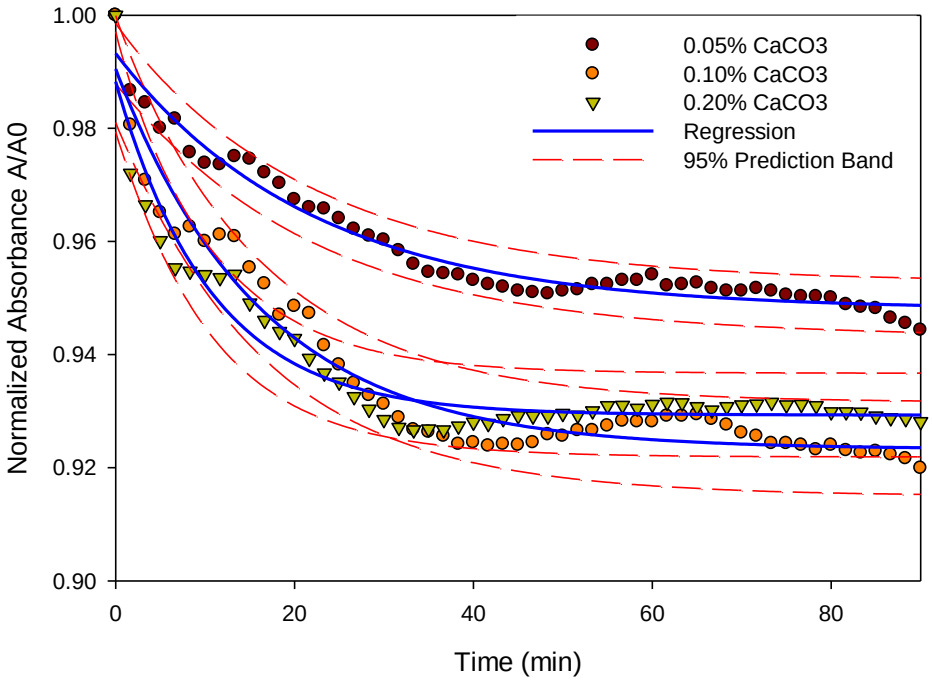

Figure 8: Normalized 90-minutes settling curve of $CaCO_3$ particles in soybean oil

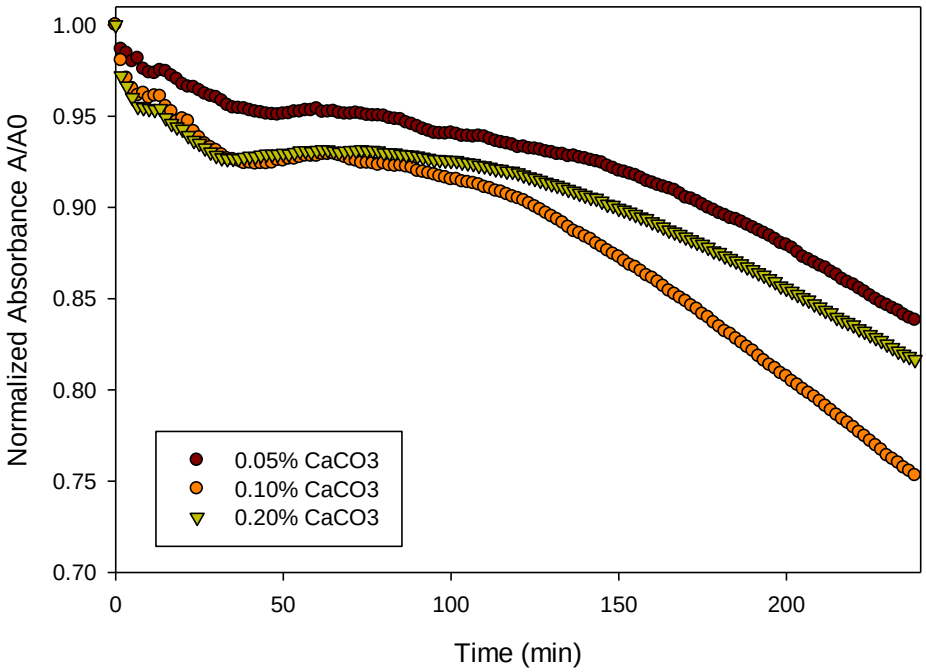

Figure 9: Normalized 4-hour settling curve of $CaCO_3$ particles in soybean oil

Table 3: Comparison of particle size on sedimentation using MgO particles

Size Fraction	MgO (% wt)	A_0 (abs)	A_1 (abs)	τ (min)
20nm	0.05	0.961 ± 0.001	0.049 ± 0.002	3.75 ± 0.352
	0.10	0.963 ± 0.001	0.046 ± 0.005	3.08 ± 0.673
	0.20	0.954 ± 0.001	0.050 ± 0.006	2.91 ± 0.600
50nm	0.05	0.945 ± 0.001	0.052 ± 0.001	5.32 ± 0.226
	0.10	0.960 ± 0.001	0.039 ± 0.001	5.61 ± 0.214
	0.20	0.979 ± 0.001	0.016 ± 0.001	72.3 ± 7.740
100nm	0.05	0.954 ± 0.001	0.041 ± 0.001	10.3 ± 0.254
	0.10	0.969 ± 0.001	0.026 ± 0.001	13.6 ± 0.685
	0.20	0.984 ± 0.001	0.014 ± 0.001	32.4 ± 2.620

Table 4: Comparison of particle loading on sedimentation using CaCO3 particles

Size Fraction	$CaCO_3$ (%wt)	A_0 (abs)	A_1 (abs)	τ (min)
~60nm	0.05	0.948 ± 0.001	0.045 ± 0.001	22.0 ± 1.50
	0.10	0.923 ± 0.001	0.067 ± 0.002	16.3 ± 1.20
	0.20	0.929 ± 0.001	0.059 ± 0.003	10.7 ± 0.83

Overall, these stability experiments allow me to conclude that 50 and 100 nm MgO and ~60 nm $CaCO_3$ particles display adequate stability in oil due to viscous effects alone for encapsulation within oil-in-water emulsions.

To analyze the effects of natural soybean oil variability on the above sedimentation results, Subtask 1.3 was completed by performing sedimentation studies of centrifuged and un-centrifuged soybean oil. The normalized absorbencies of these results are shown in Figure 10. This experiment suggests that the natural variability of the oil may contribute to the above sedimentation results because centrifuged oil displays much higher stability than un-centrifuged oil. However, the relative absorbance of the soybean oil versus the absorbance of the suspensions (shown in Figure 11) shows that this variation is slight by comparison, and is not critical enough to affect the sedimentation results. Therefore, it was concluded that the natural variability of the soybean oil did not affect the sedimentation analysis of the particle-in-oil suspensions.

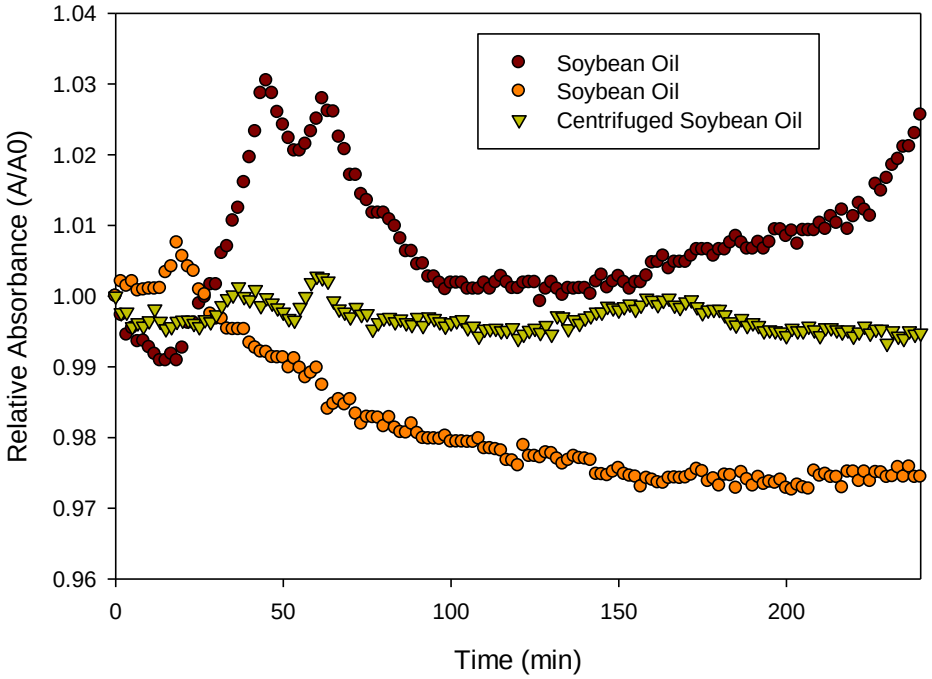

Figure 10: Normalized absorbance of centrifuged and uncentrifuged soybean oil

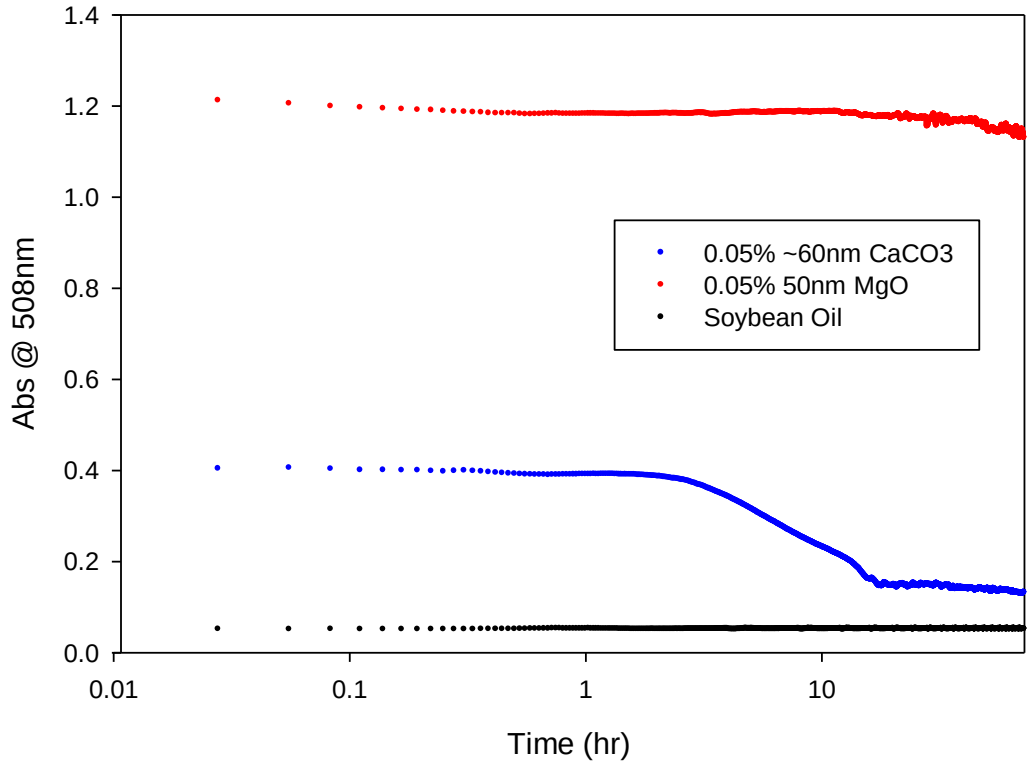

Figure 11: 72-hour sedimentation curve of 0.05% $CaCO_3$ and 0.05% MgO in soybean oil

A 72-hour sedimentation study was also conducted in order to obtain a picture of the long term settling trends of these particles. These results (Figure 11) show that MgO particles are much more stable than $CaCO_3$ particles over an extended time period. Although these results suggest that MgO particles would be the preferred particle choice for alkalinity delivery via emulsions because of their superior stability, practical considerations cannot be ignored. MgO particles are approximately twice as expensive as $CaCO_3$ particles, and therefore might be unfeasible for large-scale implantation (Sigma Aldrich).

4.2 Preliminary Alkalinity Release Rate Experiments

Since Task 1 confirmed the hypothesis that $CaCO_3$ and MgO particles would display sufficient stability in soybean oil, Task 2 was also completed. Proof-of-concept alkalinity release experiments were conducted using the methods described in Subtask 2.1. Figure 12 shows the

results of these experiments for MgO and $CaCO_3$ particles in unmodified soybean oil. These results indicate that both types of particles are indeed capable of releasing alkalinity.

Existing data of $CaCO_3$ alkalinity release from modified and unmodified soybean oil was transformed and modeled according to the methods outlined in Subtask 2.2. pH and total alkalinity (expressed as Ca^{2+} concentration) and the corresponding fit curves for this data are graphed in Figures 13 and 14, respectively. Table 5 shows the results of this analysis for soybean oil with cosolvent (1-butanol) concentrations of 0, 12.5, and 30% wt. These results suggest that the lumped mass transfer coefficient (K_l) increases as a function of cosolvent concentration. Since increased cosolvent concentration is assumed to be an indication of raised polarity, these results suggest that the lumped mass transfer coefficient increases as oil polarity increases. This verifies the hypothesis that the rate of alkalinity release can be controlled by modifying oil polarity. The Ca_{soly}^{2+} values were also empirically fit by the model. Assuming the cosolvent concentration is representative of overall oil polarity, these values do not support the hypothesis that metal solubility increases as a function of oil polarity. This hypothesis requires further exploration in Task 3.

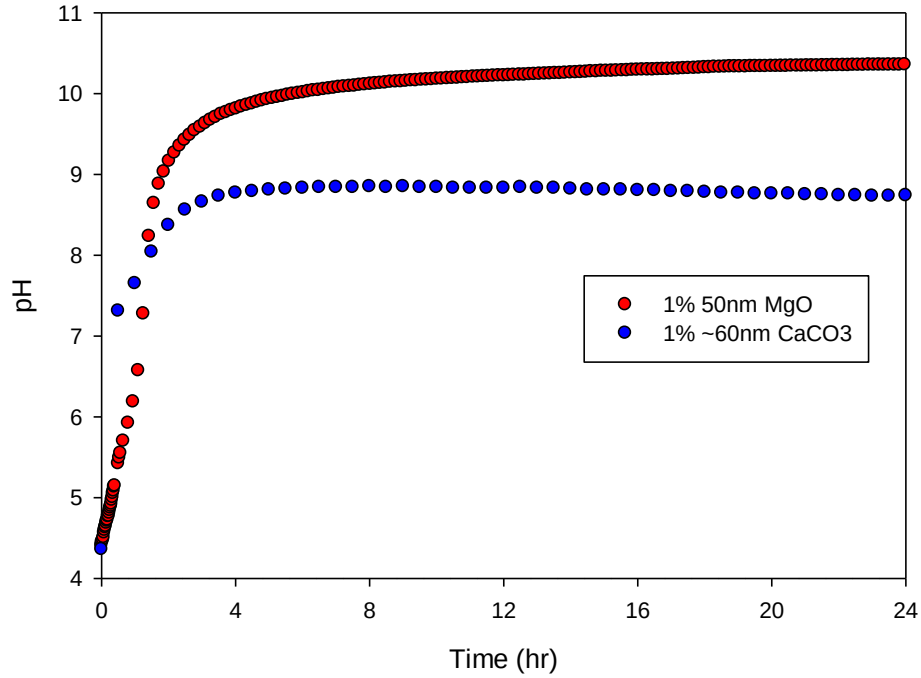

Figure 12: pH of aqueous solution vs. time, CaCO3 and MgO particles suspended in oil

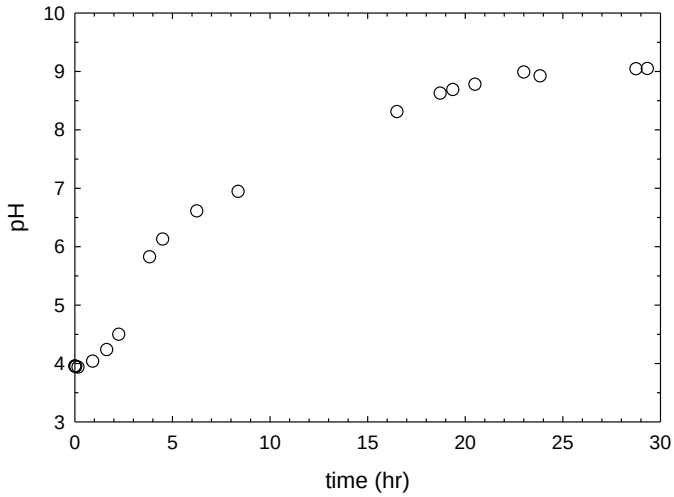

Figure 13: pH of aqueous solution vs. time & fit of CaCO3 particles suspended in oil (Data from Almquist, 2009)

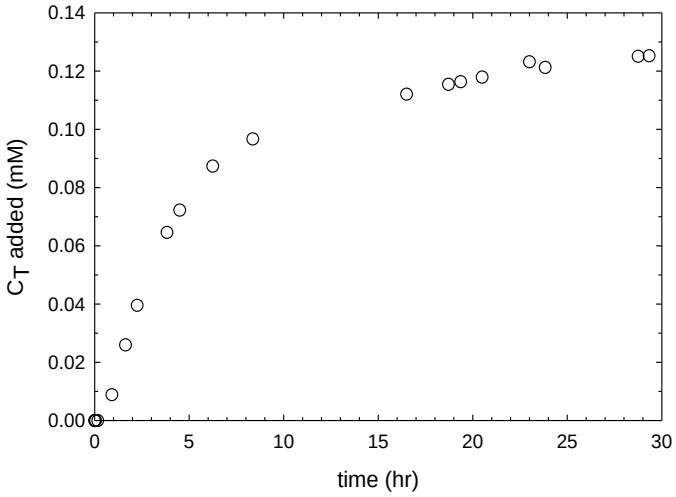

Figure 14: Representative fit (line) of pH data for $CaCO_3$ particles (Data from Almquist, 2009)

Table 5: Results of mass transfer coefficient as a function of cosolvent concentration

BuOH (% wt)	Initial pH	Ca_{soly}^{2+} (mM)	K_l (hr^{-1})
0	3.98	0.127	0.181
12.5	4.09	0.108	0.226
30	3.87	0.165	0.564

4.3 Solubility Experiments

Tasks 1 and 2 confirmed that both MgO and $CaCO_3$ particles have potential for delivery via oil-in-water emulsions. The next objective of this project was to quantify metal solubility as a function of oil polarity.

According to the methods and instrumentation described in Subtask 3.1, ICP calibration curves for aqueous and Mg^{2+} and Ca^{2+} standards were created and are shown in Figures 15 and 16. The dissolved-in-oil instrumentation described in Subtask 3.1 was refined to obtain optimization for each element for the particles-in-oil calibration curves. Instrumentation for this optimization is shown in Table 6, and the resulting calibration curves are shown in Figures 17 and 18. The R^2 values for all four calibration curves reflect sufficient accuracy for ensuing analysis of samples.

Table 6: Optimized instrumentation for dissolved-in-oil standards

Parameter	**Dissolved-in-Oil Method (Modified from Knoll and Knopp 2007)**	
	Ca^{2+}	**Mg^{2+}**
Wavelength (nm)	317.933	283.213
Plasma Flow (L/min)	18	18
Auxiliary Flow (L/min)	1.4	1.4
Nebulizer Flow (L/min)	0.45	0.45
RF wattage (W)	1500	1450
Pump Flow Rate (mL/min)	1.5	1.5

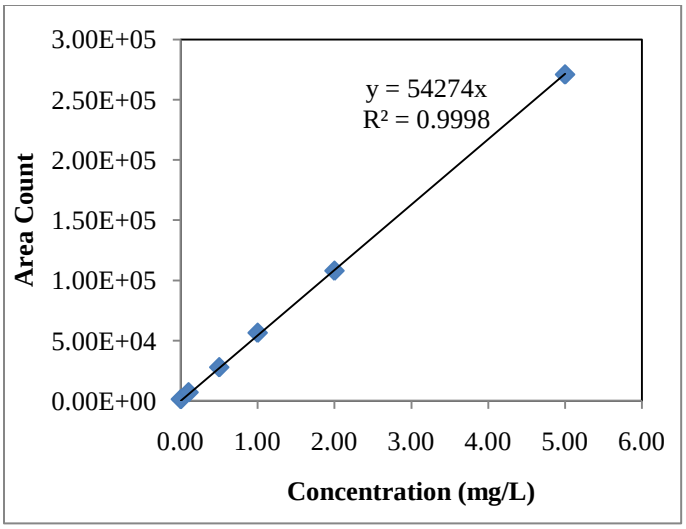

Figure 15: Aqueous Ca2+ ICP-OES calibration curve

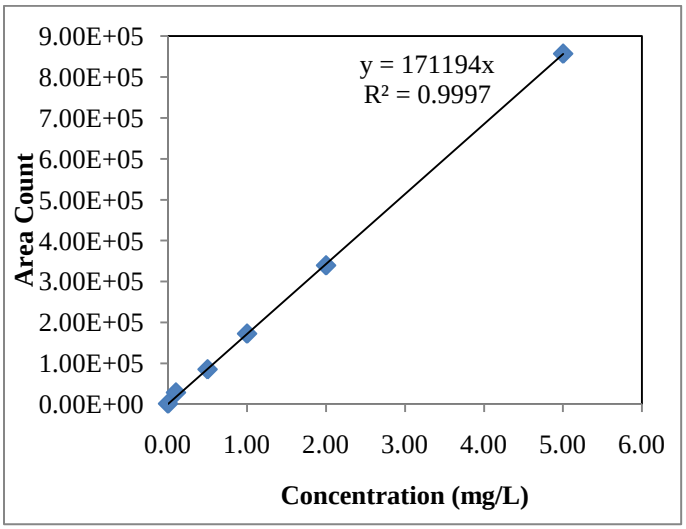

Figure 16: Aqueous Mg2+ ICP-OES calibration curve

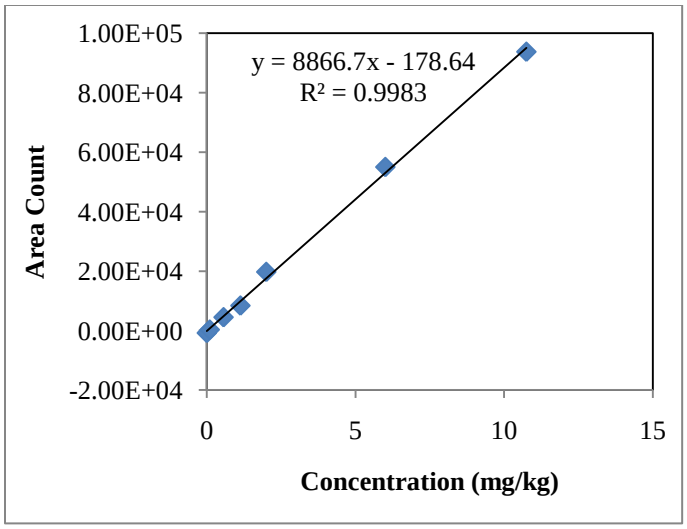

Figure 17: Dissolved-in-oil Ca2+ ICP-OES calibration curve

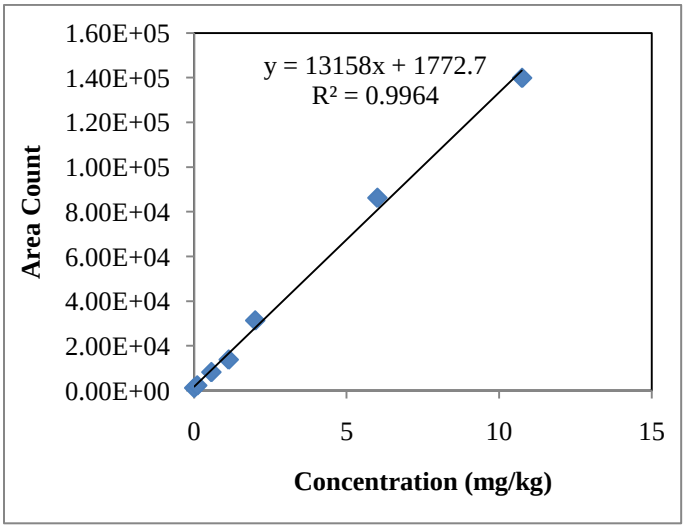

Figure 18: Dissolved-in-oil Mg2+ ICP-OES calibration curve

Figure 19 shows a plot of the 1-butanol and water content (% wt) of the modified oils that were used to complete Subtask 3.2, determining particle solubility as a function of oil polarity. Generally, the 1-butanol concentration and water content increase as oil polarity (dielectric constant) increase. However, the plot suggests that as 1-butanol concentration increases above ~2M, the dielectric constant decreases in sensitivity to increased levels of 1-butanol. This is

reflected in the large scatter of 1-butanol concentrations between dielectric constants of 5 and 5.5.

The dielectric constants of the modified soybean oils used in this subtask ranged from 3.3 (unmodified) to 5.4. The 1-butanol content of these oils ranged from 0–6 mol/L, and the water content ranged from 0–2%.

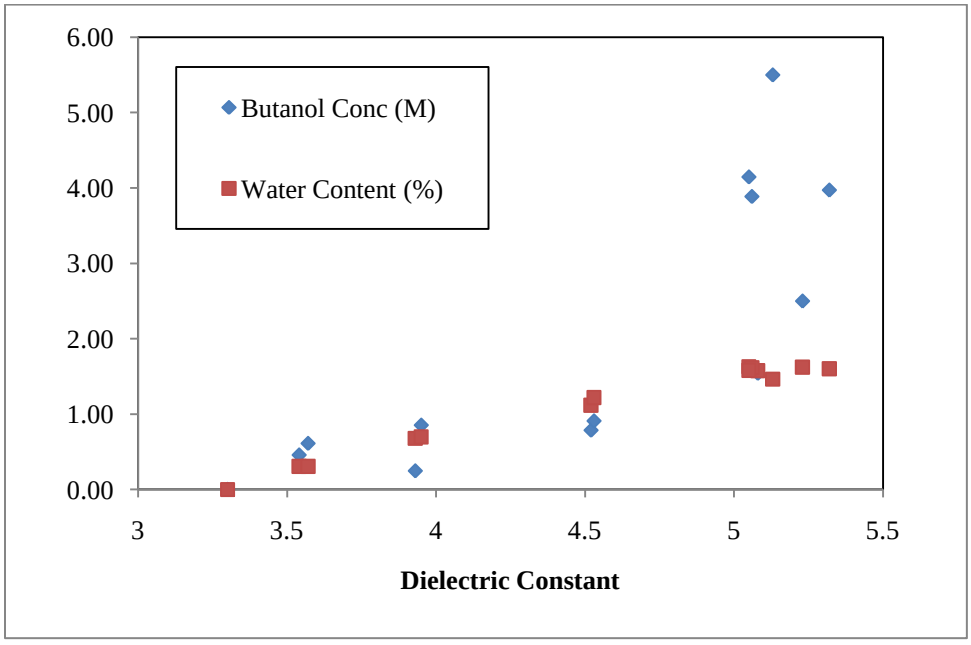

Figure 19: Properties of modified soybean oil as a function of dielectric constant

The ICP measurements were interpreted in terms of the dissolution reaction for each particle (Equations 14 and 15). For $CaCO_3$, the dissolved metal cation (Ca^{2+}) concentration is representative of the alkalinity component. The dissolved Mg^{2+} cation concentration represents half of the alkalinity component. An important distinction between these two particles is that MgO reacts with H_2O to form $Mg(OH)_2$ before the metal ion dissolves in solution.

$$CaCO_3 \rightarrow Ca^{2+} + CO_3^{2-} \quad (14)$$

$$MgO + H_2O \rightarrow Mg(OH)_2 \rightarrow Mg^{2+} + 2OH^- \quad (15)$$

Figures 20 and 21 show the results and standard deviations of the experiments outlined in Subtask 3.2, metal solubility as it relates to oil polarity, for both $CaCO_3$ and MgO particles. The solubility results below are shown in terms of the metal ion concentration in order to represent particle solubility.

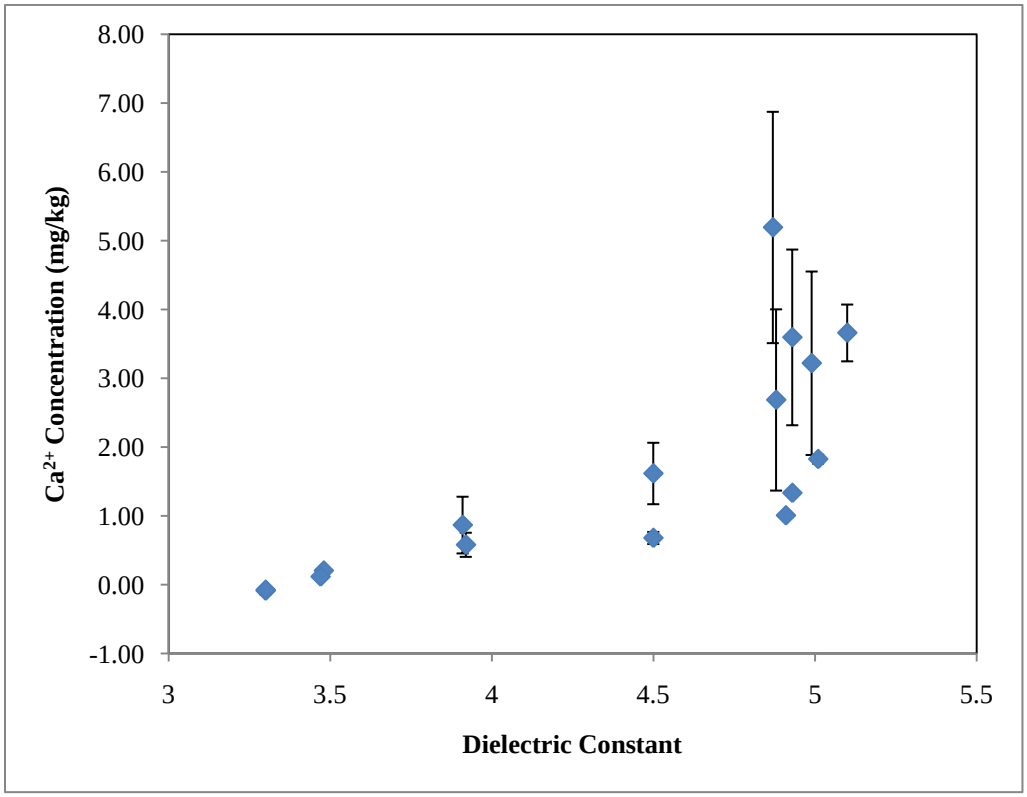

Figure 20: $CaCO_3$ particle solubility vs. oil polarity

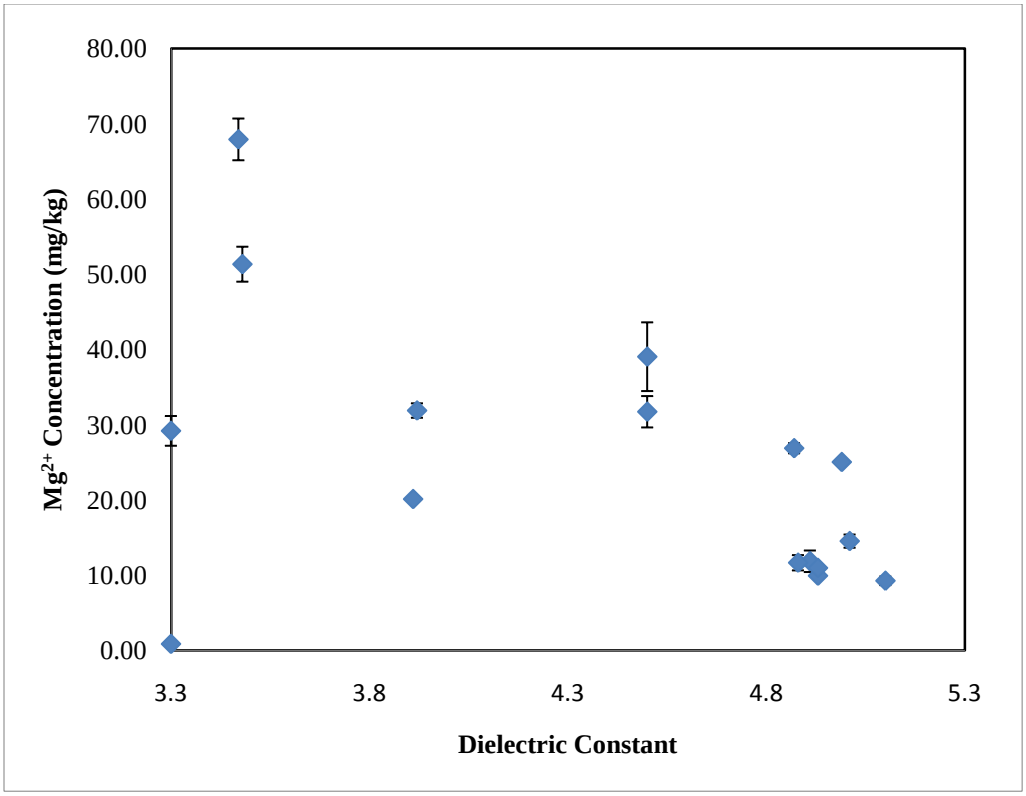

Figure 21: MgO particle solubility vs. oil polarity

These results indicate that the solubility of $CaCO_3$ particles increases as a function of oil polarity (Figure 20). Data from the studies containing MgO particles have substantial scatter, but overall trends suggest that Mg^{2+} solubility decreases as oil polarity increases (Figure 21). This observation defies a key hypothesis of this experiment and is explored further in a follow-on experiment.

This follow-on experiment was initially performed in order to determine whether the partitioning of Ca^{2+} and Mg^{2+} particles can be determined for oil-water-butanol systems as a function of oil polarity, by equilibrating butanol and soybean oil with water that has been saturated with either MgO or $CaCO_3$ particles. Figures 22 and 23 show the results of these experiments as the end metal ion concentration in the oil as a function of the end oil dielectric constant.

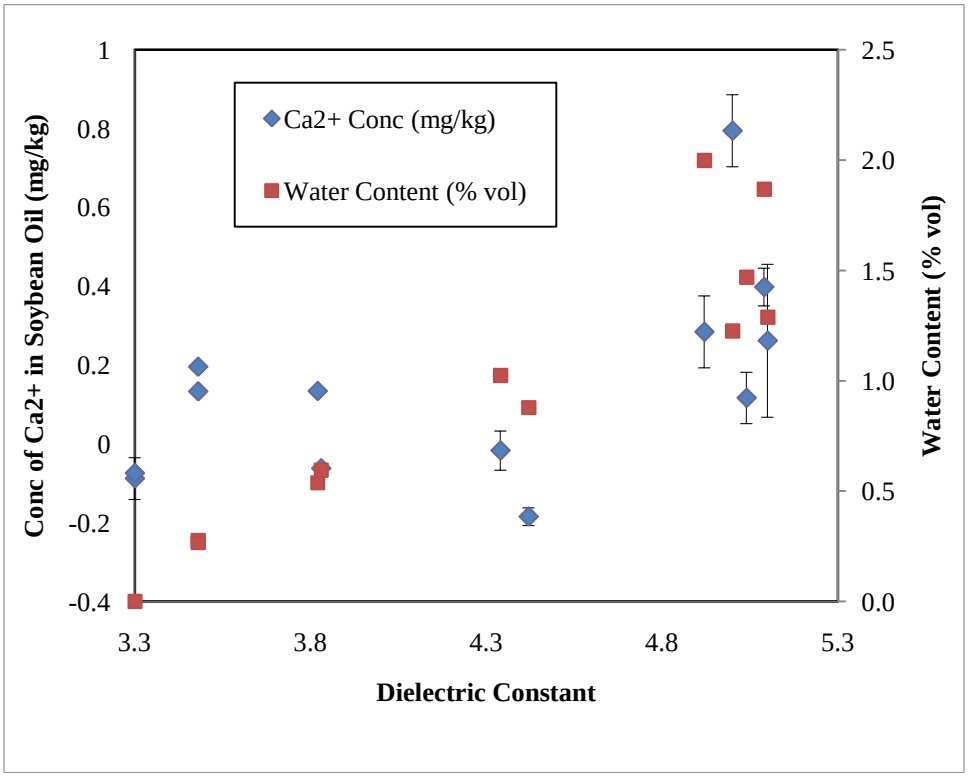

Figure 22: Ca2+ partitioning during soybean oil equilibration with water and 1-butanol

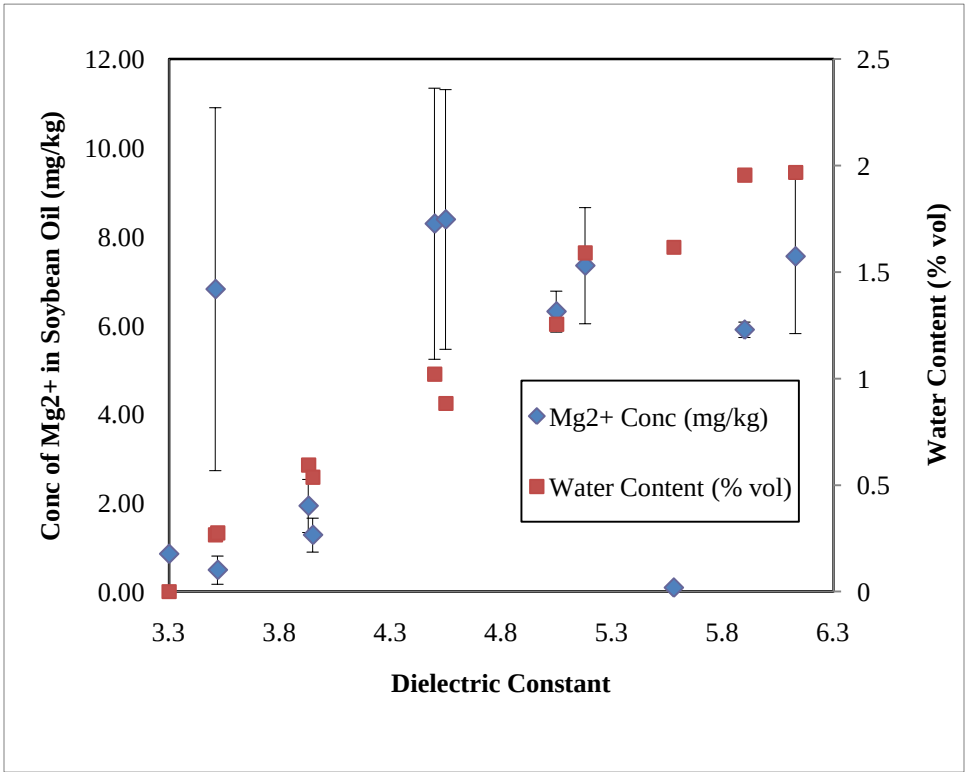

Figure 23: Mg2+ partitioning during soybean oil equilibration with water and 1-butanol

The Ca^{2+} results reveal a slight trend in that generally, the Ca^{2+} concentration in the soybean oil increases as the dielectric constant of the oil increases; however, the results have noteworthy scatter, and these Ca^{2+} concentrations are considerably lower than those found in the previous experiment (Figure 22). This plot suggests that the metal ions dissolved in the water phase are not pulled into the oil phase during equilibration.

There appears to be a trend in the Mg^{2+} solubility results for this experiment, disregarding two outliers. Although these values are also significantly lower than those found in the first solubility experiment (Figure 21), the overall trend shows Mg^{2+} solubility increasing with higher oil polarity.

To interpret these trends, volumetric water content is also shown on these plots. If Equation 15 is an accurate representation of the MgO dissolution process in these oil solutions (i.e., there are no interactions of the particles with the oil phase), the concentration of Mg^{2+} in solution should be directly proportional to the volumetric water content. Figure 23 reveals that this is not the case, as the volumetric water content increases with a linear pattern between dielectric constants of 3.3 and 5.5, and the Mg^{2+} concentrations do not. Therefore, Equation 15 is not reflective of actual dissolution processes in these oil-butanol-water systems. It may be that the long chain acids in the soybean oil are interacting with the MgO particles and are somehow interfering with the dissolution reaction described in Equation 15. This conclusion may explain the unexpected trend shown in Figure 21, where Mg^{2+} decreases as oil polarity increases.

The scattered nature of both results could be a result of the poor instrumentation of the ICP. This is reflected by the high error shown in the Mg^{2+} results (Figure 23). I recommend that these experiments be repeated with the correct ICP instrumentation, discussed below.

The Ca^{2+} solubility trends can be interpreted in the context of the kinetic model discussed in Task 2 (Equation 13). According to this model, the total carbonate concentration in solution can be determined as a function of Ca^{2+}_{soly} and the bulk mass transfer coefficient. The results of the model utilized in Task 2 showed that the mass transfer coefficient increases as a function of cosolvent concentration; whereas Task 3 showed that Ca^{2+}_{soly} increases as a function of oil polarity. Both the empirical methods of Task 2 and the experimental methods of Task 3 showed there is not a significant trend in the value of Ca^{2+}_{soly} as it relates to cosolvent concentration (Figure 24); rather, the Ca^{2+}_{soly}value is a function of overall oil polarity. The results of Task 3 reveal that cosolvent concentration is not necessarily reflective of overall oil polarity (Figure 24).

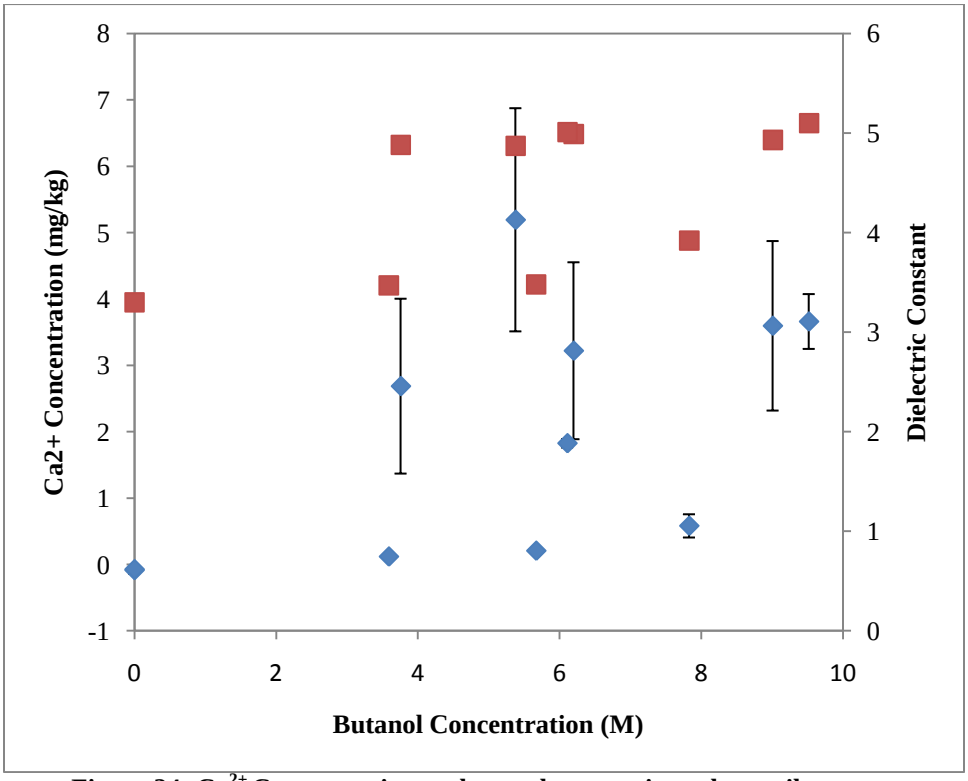

Figure 24: Ca^{2+} Concentration vs. butanol content in soybean oil

Experimental refinement would be necessary for any follow-on experiments, as it is clear that the instrument configuration used for the above experiments was not optimized for oil-based samples. The ICP-OES intensity reading varied greatly due to carbon buildup during sampling (shown in Figure 27); this is reflected by the variation in calibration curves during sampling (Figures 25 and 26, Tables 7 and 8).

To ensure sampling accuracy and to avoid excessive carbon buildup, possibly leading to equipment failure, it is recommended that any future experiments using the ICP for this purpose follow the recommendations of Perkin Elmer for spray chamber and nebulizer choice for oil-based samples. These recommendations are available in the Perkin Elmer application note: Phosphorus, Calcium, and Magnesium Analysis of Soybean Oil-Feedstock for Biodiesel Production Using the Optima ICP-OES (Knoll and Knopp, 2007).

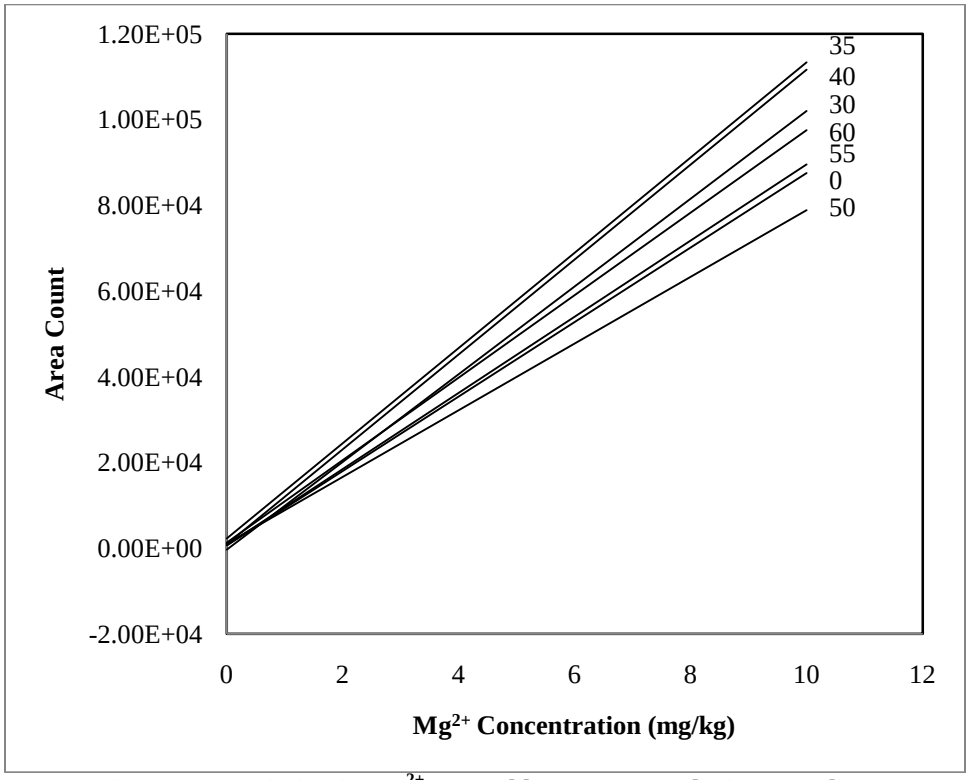

Figure 25: Variation in Mg^{2+} ICP calibration curve during sampling as a function of number of samples processed

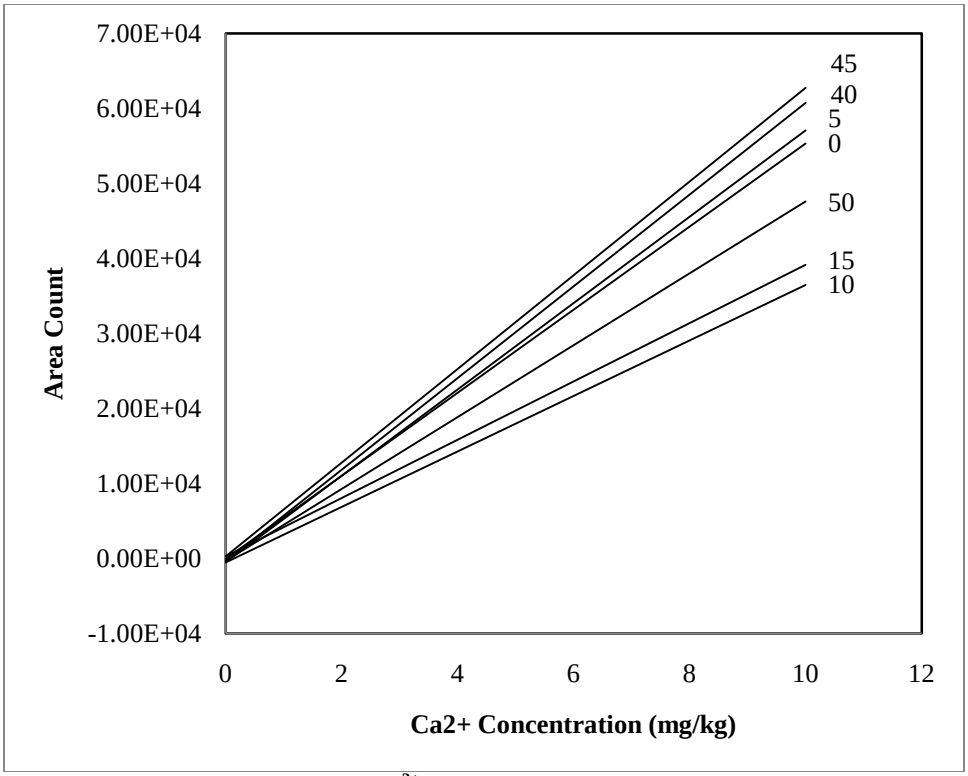

Figure 26: Variation in Ca^{2+} ICP calibration curve during sampling as a function of number of samples processed

Table 7: Variation in Ca^{2+} calibration curves during sampling

# of Samples Processed	Slope (Area-kg/mg)	Intercept (Area count)
0	5538 ± 74.16	-75.70 ± 378.2
5	5756 ± 57.52	-484.13 ± 293.3
10	3700 ± 112.2	-541.15 ± 572.3
15	3886 ± 83.44	291.37 ± 425.5
40	6114 ± 88.94	-410.24 ± 453.5
45	6244 ± 103.3	298.00 ± 527.0
50	4793 ± 22.98	-320.21 ± 117.2

Table 8: Variation in Mg^{2+} calibration curves during sampling

# of Samples Processed	Slope (Area-kg/mg)	Intercept (Area count)
0	8688 ± 44.0	632 ± 224
30	10235 ± 204	-375.1 ± 1039
35	11114 ± 164	2212 ± 836
40	11068 ± 181	911 ± 921
50	7773 ± 88.3	1072 ± 450
55	8887 ± 90.2	669.3 ± 460
60	9623 ± 144	1259 ± 733

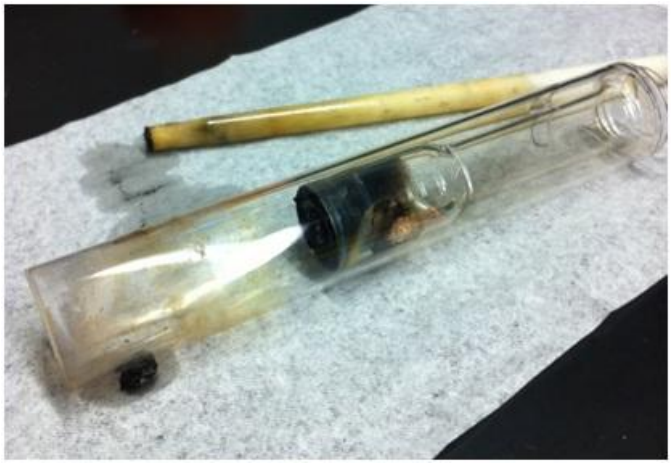

Figure 27: Carbon buildup (black residue) on ICP injector after sampling

Although some general trends can be gleaned from these solubility experiments, because of the significant scatter and large error in some of the results of Task 3, it is recommended that these experiments be repeated with the correct ICP instrumentation in order to obtain statistically significant data.

5.0 CONCLUSIONS AND RECOMMENDATIONS

Results from the experiments conducted allow me to conclude that both MgO and $CaCO_3$ particles (1) display sufficient kinetic stability in soybean oil, and (2) are capable of releasing alkalinity from an oil phase to an aqueous phase. These results indicate that both MgO and $CaCO_3$ nanoparticles have the potential to deliver alkalinity via emulsions in the subsurface. Additionally, the solubility results suggest that $CaCO_3$ particle solubility increases as a function of oil polarity. Preliminary solubility results pertaining to MgO particles suggest that the assumed dissolution reaction (Equation 15) is not reflective of actual processes in oil-butanol-water equilibrium. These solubility experiments require further refinement, as discussed in the previous section.

This research project was a small part of a larger project (NSF Grant # 1000714) aimed at a broad exploration of the mechanisms controlling emulsion-based alkalinity delivery during subsurface remediation. The conclusions from this work lay the foundation for further development of alkalinity delivery via oil-in-water emulsions. The next objective of this research is to determine how alkalinity release can be altered through modifying the solubility of metal particles in oil. I hypothesize that increasing particle solubility will increase the thermodynamic force for partitioning into the aqueous phase, thus offering control over the rate of alkalinity release. To complete this objective, Subtask 2.1 should be repeated with modified oils of varying dielectric constants, ranging from 3.3 to 6. These experiments will result in data reflecting the effects of oil polarity on alkalinity release rate. Using data obtained from experiments following the methods of Subtask 3.2, which relates oil polarity and particle solubility, future researchers will be able to determine the relationship between oil solubility and alkalinity release rate.

To further refine the alkalinity rate-of-release experiments, I suggest that future researchers proceed with the design of an experimental apparatus similar to Figure 3, but possessing a side port that accommodates the pH probe; this will avoid the probe disrupting the interfacial area and allow for more accurate analysis.

I also suggest that future follow-on experiments include alkalinity rate-of-release experiments on emulsified oil. In order to create emulsions containing either $CaCO_3$ or MgO particles, documented techniques for stabilizing emulsions that contain particles should be used (e.g., Long and Ramsburg, 2011; Almquist, 2009). Emulsions should be developed with both modified and unmodified oils. A column experiment may also be conducted to assess the emulsion transport and alkalinity release rate within a flowing system, as an extension of previous work conducted in the lab regarding emulsion encapsulation and transport (e.g., Long and Ramsburg, 2011; Berge and Ramsburg, 2009; Crocker et al., 2008). These contingent experiments would help move this research toward real-world application.

LIST OF REFERENCES

Almquist, J. 2009. Oil in Water Emulsions Containing Calcium Carbonate Particles for In Situ Neutralization of Groundwater pH. Special topics report, Department of Civil and Environmental Engineering, Tufts University, Prof. C.A. Ramsburg, advisor.

Alvarez, P.J.J and W.A. Illman. 2006. Bioremediation and Natural Attenuation. Wiley-Interscience, p. 609.

Arcadis. 2002. Technical Protocol for Using Carbohydrates to Enhance Reductive Dechlorination of Chlorinated Aliphatic Hydrocarbons. Report prepared for ESTCP (Contract #F41624-99-C-8032).

Aulenta F., Majone M., Tandoi V. 2006. Enhanced anaerobic bioremediation of chlorinated solvents: Environmental factors influencing microbial activity and their relevance under field conditions. *Journal of Chemical Technology and Biotechnology*, 81: 1463–1474.

Berge, N.D. and C.A. Ramsburg. 2009. Oil-in-water emulsions for encapsulated delivery of reactive iron particles, *Environmental Science and Technology*, 43(13): 5060–5066.

Bialkowski, S. "Carbon Dioxide – Carbonic Acid Equilibrium." 2004. Department of Chemistry and Biochemistry, Utah State University. < http://www.chem.usu.edu> (Viewed January 24, 2011).

Borden, R.C. 2007. Effective Distributive of Emulsified Edible Oil for Enhanced Anaerobic Bioremediation, *Journal of Contaminant Hydrology*, 94: 1–12.

Borden, R.C., M. Clayton, A. Weispfenning, T. Simpkin, and M.T. Lieberman. 2008. Emulsified Oil Design Tool: User's Manual, Environmental Security Technology Certificate Program, North Carolina State University.

Coulibaly, K.M. and R.C. Borden, 2004. Impact of Edible Oil Injection on the Permeability of Aquifer Sands. *J. Contaminant Hydrology*, 71(1-4): 219-237.

Crocker, J.J., N.D. Berge, and C.A. Ramsburg. 2008. Encapsulated delivery of reactive iron particles using oil-in-water emulsions. In: GQ07: Securing Groundwater Quality in Urban and Industrial Environments, Ed. Trefry, M.G., IAHS Publication No. 324: 242–249.

Deutsch, W. J., M. Dooley, S. Koenigsburg, B. Butler and G. Dobbs, 2002. "In Situ Redox Manipulation for Arsenic Remediation." Proceedings of the Third International Conference on Remediation of Chlorinated and Recalcitrant Compounds (Monterey, Calif. May 20-23, 2002.) Battelle Press, Columbus, Ohio.

"Dielectric Constants Chart." Technical document, ASI Instruments. <http://www.asiinstr.com> (Viewed January 24, 2011).

Dragun, J. 1988. The Soil Chemistry of Hazardous Materials. Hazardous Materials Control Research Institute, Silver Springs, Md.

EN 14538: Fat and oil derivatives – Fatty acid methyl ester (FAME) – Determination of Ca, K, Mg and Na content by optical emission spectral analysis with inductively coupled plasma (ICP OES). 2006. British Standard Institution.

Enfield, Carl et al. 1999. In Situ Enhanced Source Removal. EPA 600-C-99-002.

Knoll, R. and M. Knopp. 2007. Phosphorus, Calcium, and Magnesium Analysis of Soybean Oil-Feedstock for Biodiesel Production Using the Optima Inductively Coupled Plasma-Optical Emission Spectrometer (ICP-OES). Application note; Perkin Elmer, Inc.

Marlow, C. 2009. EOS Remediation: In Situ Remediation Using EOS® and AquaBupH®. Center for Environmental Studies.

Harned, H.S. and S.R. Scholes, Jr. 1941. The First Ionization Constant of HCO_3—From 0 to 50º. *J. Amer. Chem. Soc.*, 63: 1706-1709.

Harned, H.S. and W.J. Hamer. 1933. The Ionization Constant of Water and the Dissociation of water in Potassium Chloride Solutions from Electromotive Forces of Cells Without Liquid Juntion. *J. Amer. Chem. Soc.*,55: 2194-2206.

Hydrochloric Acid; MSDS. May 2010. Seastar Chemicals Inc. <http://wwwsci.seastarchemicals.com/> (Viewed January 24, 2011).

Lee, W. and B. Batchelor. 2002. Abiotic Reductive Dechlorination of Chlorinated Ethylenes by Iron-Bearing Soil Minerals, *Environmental Science and Technology*, 36: 5348–5354.

Long, C. M., and R. C. Borden. 2006. Enhanced Reductive Dechlorination in Columns Treated with Edible Oil Emulsion, *J. Contaminant Hydrology*, 87: 54–72.

Long, T. and C.A. Ramsburg. 2011. Encapsulation of nZVI Particles using a Gum Arabic Stabilized Oil-In-Water Emulsion, *Journal of Hazardous Materials.*

Lutes, C. C., A. Frizzell, and S. S. Suthersan. 2006. "Enhanced Reductive Dechlorination of CAHs using Soluble Carbohydrates--A Summary of Detailed Data from 50 Sites." Principles and Practices of Enhanced Anaerobic Bioremediation of Chlorinated Solvents, Appendix E. AFCEE/NFESC/ESTCP, Brooks City-Base, TX.

McClements, D.J., E.A. Decker, and J. Weiss. 2007. Emulsion-based delivery systems for lipophilioc bioactive components. *Journal of Food Science,* 72: R109–R124.

McDade, Travis and Newell. 2005. Analysis of DNAPL source-depletion costs at 36 field sites, *Remediation Journal*, 15: 9–18.

Nicolosi, V., D. Vrbanic, A. Mrzel, J. McCauley, S. O'Flaherty, C. McGuinness, G. Compagnini, D. Mihailovic, W. Blau, and J. Coleman. April 2005. "Solubility of $Mo_6S_{4.5}I_{4.5}$ Nanowires in Common Solvents: A Sedimentation Study," *Journal of Physical Chemistry B,* 109: 7124–7133.

Phenrat, T., N. Saleh, K. Sirk, H.J. Kim, R.D. Tilton, G.V. Lowry. 2008. Stabilization of Aqueous Nanoscale Zerovalent Iron Dispersions by Anionic Polyelectrolytes: Adsorbed Anionic Polyelectrolyte Layer Properties and their Effect on Aggregation and Sedimentation. J. *Nanoparticle Res*, 10: 795–814.

Ramsburg, C.A., K.D. Pennell, T.C.G. Kibbey, and K.F. Hayes. 2003. Use of a Surfactant-Stabilized Emulsion to Deliver n-Butanol for Density Modified Displacement of Trichloroethene-NAPL. *Environ. Sci. Technol*., 37(18): 4246–4253.

Ramsburg, C.A., J. Almquist, O. Leach. 2011. Exploration of the Mechanisms Controlling Emulsion-Based Alkalinity Release during Subsurface Remediation. Proceedings of 2011 NSF Engineering Research and Innovation Conference, Atlanta, Georgia. Department of Civil and Environmental Engineering, Tufts University.

Robinson, C. and D.A. Barry. 2009. Design tool for estimation of buffer requirement for enhanced reductive dechlorination of chlorinated solvent in groundwater. *Environmental Modeling & Software*, 24: 1332–1338.

Sarojam, P. 2010. Analysis of Trace Metals in Surface and Bottled Water with the Optima 7300 DV ICP-OES. Application note; PerkinElmer, Inc.

Shadlovsky, T. and D. McInnes, 1935. The Ion Activity Coefficient Product and Ionization of Water in Univalent Halide Solutions—A Numerical Study. *J. Amer. Chem. Soc.*, 59: 2304-2305.

Vainberg, S., R.J. Steffan, R. Rogers, T. Ladaa, D. Pohlmann and D. Leigh. 2006. *Production and Application of Large-Scale Cultures for Bioaugmentation,* The Fifth International Remediation of Chlorinated and Recalcitrant Compounds Conference, Monterey, CA.

Verstraete, W., Vanloocke, R., de Borjer, R., and Verlinde, A. 1976. Modeling of the Breakdown and the Mobilization of Hydrocarbons in Unsaturated Soil Layers, in *Proceedings of the 3rd International Biodegradation Symposium,* Applied Science, London, 99–112.

Wu, W-M., J. Carley, M. Fienen, T. Mehlhorn, K. Lowe, J. Nyman, J. Luo, M.E. Gentile, R. Rajan, D. Wagner, R.F. Hickey, B. Gu, D. Watson, O.A. Cirpka, P.K. Kitanidis, P.M. Jardine, and C.S. Criddle. 2006. Pilot-scale in situ bioremediation of uranium in a highly contaminated aquifer. 1. Conditioning of a treatment zone. *Environmental Science and Technology*, 40(12): 3978–3985.

APPENDIX A

Table 9: Instruments used in experiments

Instrument	Manufacturer	Model
UV/VIS Spectrophotometer	PerkinElmer	Lambda 25
pH meter	Mettler-Toledo	Seven Multi
Inductively Coupled Plasma Optical Emission Spectrophotometer	PerkinElmer	Optima 7300 DV
Gas Chromatograph	Hewlett-Packard	Series II 5890
Headspace Sampler	PerkinElmer	Turbomatrix 40 Trap
Gas Chromatograph	Hewlett-Packard	6890 Series
Dielectric Constant Meter	Brookhaven	BI-870
Karl Fischer Titrator	Mettler-Toledo	DL38
Centrifuge	Beckman Coulter	Avanti J-25
Sonic Dismembrator	Fisher Scientific	500

Table 10: Materials used in experiments

Material			Manufacturer	Grade	Physical Properties	
					Dielectric Constant (25°)	Bulk Density (g/cm^3)
Calcium Carbonate particles	99%+ purity	60nm[4]	Acros Organics	ACS	N/A	2.83
	98% purity	10µm	Sigma-Aldrich			2.93
Magnesium Oxide particles, 99%+ purity		20nm	Nanostructured & Amorphous Materials, Inc.	ACS	N/A	3.58
		50nm				
		100nm				
		~44µm	Sigma-Aldrich			
1-Butanol			Fisher Scientific	HPLC	17.8[5]	0.81
Hydrochloric acid			Fisher Scientific	HPLC	78.30[6]	1.18
Milli-Q water			Millipore	N/A	80.4[1]	0.845-0.875
Soybean oil			MP Biomedicals	Laboratory	3.3[1]	0.92
Kerosene			Sigma Aldrich	Pure	1.8[1]	0.81
Calcium and Magnesium Dissolved in Oil ICP-OES Calibration Standard			AccuStandard	Pure	N/A	N/A
Calcium ICP-OES Calibration Standard, Matrix: 2% HNO_3			PerkinElmer	Pure	N/A	N/A
Magnesium ICP-OES Calibration Standard, Matrix: 2% HNO_3			PerkinElmer	Pure	N/A	N/A
1% Water Standard			AQUASTAR	Reagent	N/A	1.00

[4] Almquist, 2009
[5] "Dielectric"
[6] Hydrochloric, 2010

VITA

Olivia Leach grew up in Darien, Connecticut with her parents and two older sisters. She graduated from Darien High School in 2007 where she ran varsity track.

Olivia enrolled in Tufts University in the fall of 2007, where she became involved in the Integrated Multiphase Environmental Systems Laboratory, first as a research assistant, and then to conduct her own thesis research. In 2010, she was the recipient of a John A. Cataldo award from the Department of Civil and Environmental Engineering. Her time at Tufts helped her develop a strong interest in environmental health, and also included work at the Student Outreach Mentorship Program, during which she volunteered at a local school to teach elementary school children about engineering. She was also a member of the Tufts sailing team and knitting club, and spent a fair amount of time skiing in Vermont.

Next year, Olivia is enrolling at Emory University's Rollins School of Public Health to pursue a Master's in Public Health in Environmental Health. Olivia hopes to eventually apply her combination of Environmental Engineering and Environmental Health studies through public surface elsewhere in the world, and possibly join the Peace Corps.